Simulation of Hot Forming Processes of Refractory Metals using Porous Metal Plasticity Models

Erik Parteder*, Hermann Riedel+, Dong-Zi Sun+

*Plansee AG, Reutte, Tyrol, Austria

+Fraunhofer Institute for Mechanics of Materials, Freiburg, Germany

Summary

In this work two models for predicting the densification behavior of sintered refractory metals during hot working operations are presented. It is known from experiments and cell model calculations that the pore shape change has a significant influence on the densification behavior. Therefore this effect should be included in a continuum constitutive description. The first model presented is a phenomenological extension of the Gurson model, the second one is the model of Gologanu, Leblond & Devaux, which was implemented as a user material model into the Finite-Element-code ABAQUS. The numerical results are compared with the density distribution of a tapered disk made of pure molybdenum after the hot forming operation.

Keywords

Porous Metal Plasticity, FE-Simulation, Hot Forming

1. Introduction

Hot working of refractory metals after the sintering procedure aims at achieving the desired shape and mechanical properties and to eliminate the porosity. Therefore understanding of the densification behavior of the porous metals during the hot forming operation is of great importance for process design and process optimization.

The presence of pores in sintered parts requires that pressure-dependent, dilatant constitutive laws are used to model hot forming operations on these materials. The porosity (or the relative density), is treated as an internal variable.

In the past a large number of phenomenological as well as micromechanics based constitutive laws for porous materials were developed. The first phenomenological yield functions for porous media (Kuhn & Downey 1971, Shima & Oyane 1976) assume isotropic response at yielding even for finite plastic deformation. The only microstructural feature is the relative density. Some models originate from the continuum damage theory of ductile materials, the well-known Gurson model (Gurson 1977), extended by Tvergaard (1981), being one of them. Gurson's model assumes that the pore shape is spherical at the beginning as well as throughout plastic deformation, and therefore the mechanical behavior remains also isotropic. The material behavior of the matrix is assumed to be perfectly plastic. Isotropic constitutive laws for linear and nonlinear viscous materials were also developed and applied to hot isostatic pressing simulations (Duva & Hutchinson 1984).

More recently, Gologanu et al. (1993, 1994) generalized the Gurson model to include the evolution of the pore shape during plastic deformation. The pore aspect ratio is an internal variable, and the stress-strain response becomes anisotropic as the pores develop prolate or oblate shapes. An alternative approach based on a constitutive theory for particulate composites was proposed by Ponte Castañeda & Zaidman (1994).

In the present work two approaches of continuum-models describing the densification behavior of sintered refractory metals are presented. The first one is a modification of the Gurson model (referred as model 1), by introducing evolution equations for the parameters q_1 and q_2 proposed by Tvergaard, with the restriction that the influence of the pore shape change on densification is incorporated in a phenomenological manner (the model remains isotropic). The parameters of the evolution equations for q_1 and q_2, are fitted to experimental results (uniaxial stress state) and axisymmetric unit cell calculations (stress states with arbitrary triaxialities). The advantage of this model is that different microstructural features which characterize the material (like the local distribution of the pores within the matrix or the effect of different pore sizes) can be taken into account in an overall manner. The disadvantage is that the model is applicable strictly only for proportional loading conditions (no change of triaxiality during plastic straining).

As a second approach, we have implemented the model of Gologanu et al. (1993, 1994) as a user defined material model in the FE-code ABAQUS (referred as model 2) (Andrieux et al. 2000).

The advantage of this model is that it describes the evolution of the pore shape and of the anisotropic material response consistently, based on reliable models for void growth and void deformation. Hence a much wider range of validity is expected than for model 1. For example, data measured in uniaxial compression can be applied with greater confidence to forming operations where the stress triaxiality may be much higher. In its present form the model neglects possible rotations of the principal axes of the pores.

2. Experiments

Green compacts with different green densities were produced from pure molybdenum powder by applying different compaction pressures. All samples were sintered in one batch. The same temperature history implies that the grain size is the same in all samples, and only the relative density varies due to the different densities of the green parts. This means, that the mechanical behavior after sintering depend on the density only.

The sintered samples were tested in uniaxial compression at a temperature of 1000°C. One set of samples (diam. 5 mm and height 6 mm) were deformed up to a plastic strain of $\varepsilon \approx 1$ to evaluate the stress-strain-behavior. The relative densities of this set ranges from $D_0 = 0.917$ to 0.96. The samples of the second set (diam. 12 mm and height 14.4 mm) with initial relative densities of $D_0 = 0.92$, 0.94 and 0.96 are compressed to different heights, in order to measure the relative density after a certain amount of plastic strain with the Archimedes method. Details are described in Parteder et al. (1999). Additional compression tests on tapered disks for verification of both models are described in section 5.

3. The Gurson model and its modification

Gurson's yield function was derived from an upper bound solution of the velocity field of a hollow sphere or a shell with an incompressible shell material. The flow potential Φ has the form

$$\Phi = \frac{\sigma_e^2}{\sigma_M^2} + 2q_1 \cosh\left(\frac{3q_2\sigma_h}{2\sigma_M}\right) - \left[1 + q_3(1-D)^2\right], \tag{1}$$

where σ_M denotes the matrix flow stress, D is the relative density defined as ϱ/ϱ_M, where ϱ is the density of the porous metal and ϱ_M is the density of the matrix material, σ_e is the equivalent stress of the porous continuum and σ_h is the hydrostatic stress. q_1, q_2 and q_3 are the parameters proposed by Tvergaard. He suggested values of $q_1 = 1.5$, $q_2 = 1$ and $q_3 = q_1^2$. For all further calculations we also use the relation $q_3 = q_1^2$. Note that for $q_1 = q_2 = q_3 = 1$ the original Gurson model is recovered and that for $D = 1$, which means that the material is fully dense, the Mises yield condition is gained.

The constitutive model is completed by the argument that normality of the matrix material implies normality of the porous continuum (Berg 1970)

$$d\varepsilon_{ij} = d\lambda \frac{\partial \Phi}{\partial \sigma_{ij}} . \tag{2}$$

3.1. Uniaxial stress state

As a first step the uniaxial stress state is investigated. The modification of Gurson's model is attained by considering the parameters q_1 and q_2 as internal variables representing the influence of the pore shape in a manner which is not explicitly specified. The evolution of q_1 and q_2 is linked to the equivalent plastic strain of the porous metal and the following equations are proposed

$$q_1 = q_1^0 \left(1 + \frac{\varepsilon_e}{\bar{\varepsilon}_1}\right)^{n_1}, \quad q_2 = q_2^0 \left(1 + \frac{\varepsilon_e}{\bar{\varepsilon}_2}\right)^{n_2}, \tag{3}$$

where ε_e is the equivalent plastic strain of the porous material, q_1^0 and q_2^0 are the initial parameters for zero plastic strain, $\bar{\varepsilon}_1$, $\bar{\varepsilon}_2$, n_1 and n_2 are constants which will be determined by a best fit with the experimental results, see table 1 below.

For uniaxial compression the yield condition, $\Phi = 0$, with Φ from equation 1 gives the yield stress σ_y of the porous metal

$$\sigma_y = \sigma_M \frac{2\left[1 - q_1 (1 - D)\right]}{\left[4 + q_1 q_2^2 (1 - D)\right]^{1/2}} . \tag{4}$$

The evolution of the density is related to the volumetric strain increment, which is obtained from equation 2. For uniaxial compression it follows

$$dD = -\frac{3D\, q_1 q_2^2 (1 - D)}{4 + q_1 q_2^2 (1 - D)} d\varepsilon , \tag{5}$$

where ε is the component of the plastic strain along the compressive axis. Equation 5, together with equation 3 is integrated numerically using computer algebra. This gives relations for the yield stress $\sigma_y = \sigma_y(D,\varepsilon)$ and for the evolution of the density $D = D(\varepsilon)$. Figures 1 and 2 show the results of the

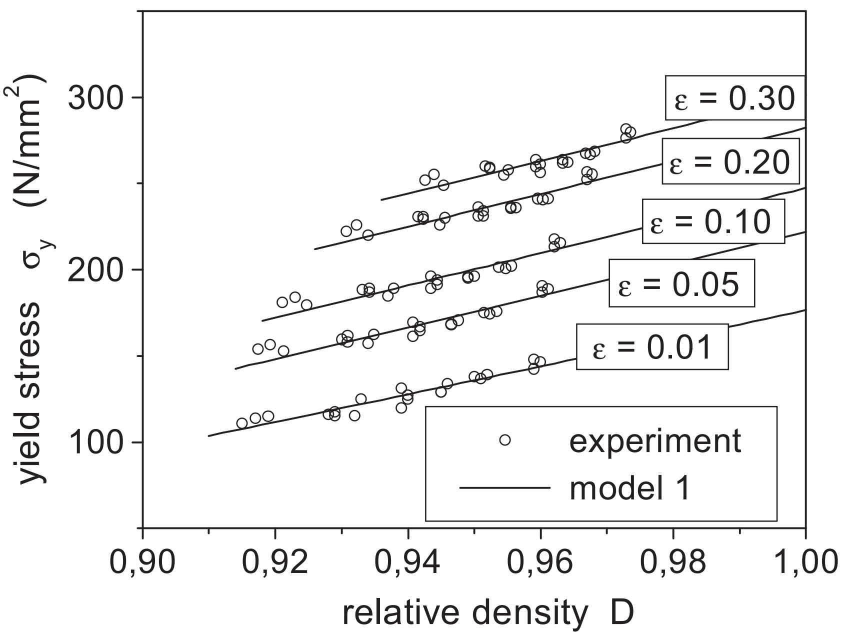

Figure 1. Yield stress of the porous metal versus relative density for different levels of plastic strain; experiments (uniaxial compression) compared with the modified Gurson model (model 1).

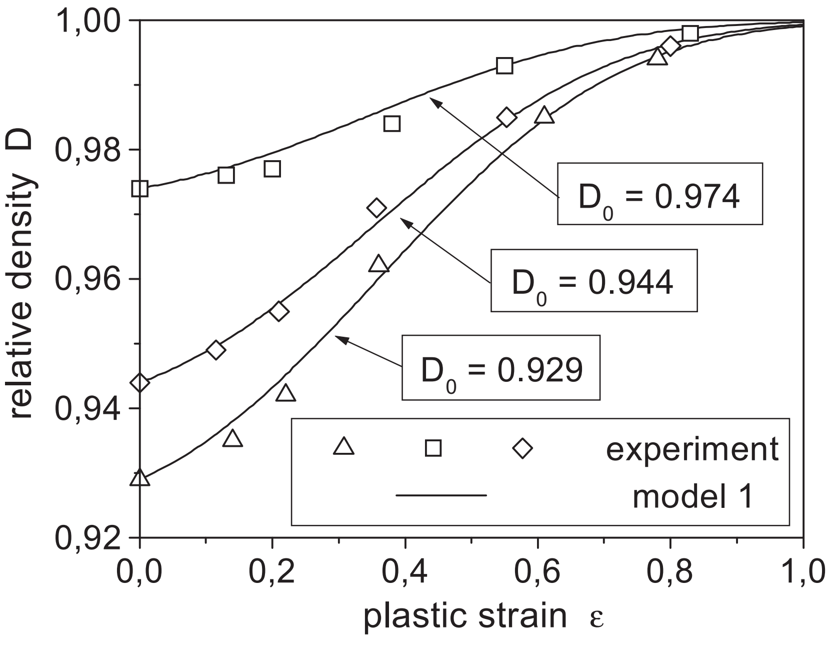

Figure 2. Density evolution in uniaxial compression for different initial densities; experiments compared with the modified Gurson model (model 1).

integration adjusted to the experimental results, and table 1 shows the values of the parameters resulting from the best fit.

$q_1^0 = 4.66$	$\bar{\varepsilon}_1 = 0.1$	$n_1 = -0.75$
$q_2^0 = 0.45$	$\bar{\varepsilon}_2 = 0.2$	$n_2 = 1.25$

Table 1. Parameters of equation 3 for the uniaxial stress state.

3.2. Arbitrary compressive stress states

For arbitrary compressive stresses experimental data are hard to obtain. Instead, micromechanical cell model calculations are a suitable method to get reasonable results for characterizing the densification behavior of the porous metal. In our case simple axisymmetric cell models with symmetric boundary conditions were used (Parteder 2000).

Figure 3 shows the simplification of a porous solid, assuming a regular cubic pore arrangement and the approximation of a hexaedron with a cylinder. For a given triaxiality, which is defined as $X = \sigma_h / \sigma_e$, the ratio of the axial load σ_z and the radial component σ_r can be calculated as

$$\begin{aligned} \frac{\sigma_r}{\sigma_z} &= \frac{3X+1}{3X-2} \quad \rightarrow \quad \text{"sphere to crack"}, \\ \frac{\sigma_z}{\sigma_r} &= \frac{3X+2}{1-3X} \quad \rightarrow \quad \text{"sphere to needle"}. \end{aligned} \tag{6}$$

Note that for axisymmetric stress states we have to distinct between the evolution of oblate and prolate pore shapes. In the first case the full densified state is a penny shaped crack, starting from a spherical pore, the evolution is reffered as „sphere to crack“. The prolate pore shapes evolve from „sphere to needle“.

The densification characteristic of the cell can be computed from the displacement vector of the edge node of the cell. In order to fit the modified Gurson model to these cell model calculations the parameters q_1 and q_2 were assumed to depend on the stress triaxiality in addition to the dependence on the plastic strain specified in equation 3

$$q_1 = q_1(\varepsilon_e, X), \quad q_2 = q_2(\varepsilon_e, X). \tag{7}$$

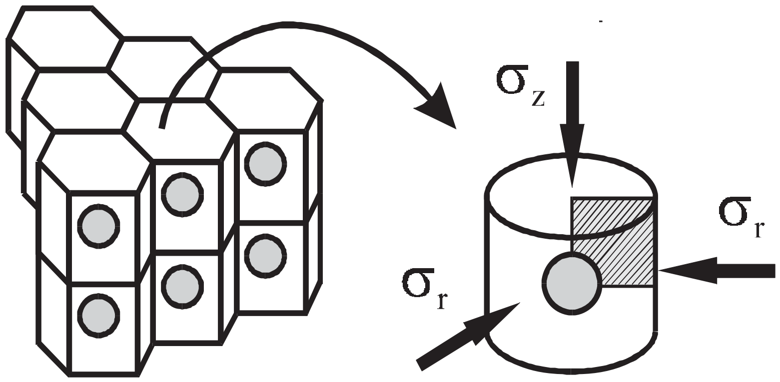

Figure 3. Sketch of regular pore arrangement and the extraction of a axisymmetric unit cell.

The functional form of equation 7 is given in Parteder (2000). The above relation is only valid for proportional loading conditions, because it is assumed that the change of the triaxiality during loading will influence the pore shape evolution and therefore the density evolution.

Figure 5 below shows the density evolution for various triaxialities as predicted by cell models, by the modified Gurson model and by the Gologanu model.

4. Gologanu model and its implementation as a user defined material model

The model of Gologanu et al. is a generalization of the Gurson model. In addition to the relative density D, which is the only state variable in the flow potential of the Gurson model, the model of Gologanu et al. contains a pore shape variable S as a second state variable. If a and b are the semi-axes of a spheroidal pore (a is the semi-axis in axial direction, b is the semi-axis in radial direction), S is defined as $S = \ln(a/b)$. Prolate pores have $S > 0$, oblate pores are characterized by $S < 0$, and spherical pores by $S = 0$.

The material model exhibits an evolving anisotropy depending on the orientation of the axes of the pore and on the value of S. The functional form of the flow potential is given as

$$\Phi = C\frac{\sigma_e^{*2}}{\sigma_M^2} + 2q_1^*\,(g+1)(g+1-D)\cosh\left(\frac{\kappa\sigma_h}{\sigma_M}\right) - (g+1)^2 - q_1^{*2}(g+1-D)^2. \qquad (8)$$

The parameters C, κ, and g are dependent on the pore shape parameter S and the relative density ($g = 0$ for prolate and spherical pores). σ_e^* is a modified equivalent stress, dependent on the internal variables. The Tvergaard parameter q_1^* in this case is also dependent on the the pore shape. The evolution of the pore shape is given by the relation

$$\dot{S} = S_a \dot{\varepsilon}_z' + S_b \dot{\varepsilon}_h , \tag{9}$$

where the parameters S_a and S_b are functions on the stress triaxiality and the pore shape. $\dot{\varepsilon}_z'$ is the deviatoric part of the plastic strain rate in direction of the axis a (axial or z-direction) and $\dot{\varepsilon}_h$ is the volumetric strain rate. The model of Gologanu et al. was coded in Fortran for arbitrary uniform straining histories (with no spatial dependence) and as a user subroutine for the FE-code ABAQUS/Explicit. Special care must be expended for spherical pores (when the pore shape parameter of the model is $S = 0$ and expressions of the form $\infty - \infty$ occur), and for crack- or needle-like pores (when $S = \pm\infty$). Euler forward integration is used throughout, including the yield condition, which is treated as $d\Phi = 0$. Concerns that the stress state could drift away from the yield surface, if only the incremental form of the yield condition is used, proved to be unnecessary. With the small time steps that are chosen by an explicit code the deviation from the yield surface usually remained smaller than 1% and is probably not larger than other inevitable inaccuracies of the time integration scheme.

Figure 4 shows the yield stress of the porous metal in dependence on the relative density for different levels of plastic strain. The results for the modified Gurson model (model 1) and the Gologanu model (model 2) are compared with the original Gurson model (model 1 gives the best coincidence with the experimental results). One can see the increasing drop of the yield stress predicted by model 2 due to the evolving anisotropy. Figure 5 shows the evolution of the density for two different stress triaxialities. For the uniaxial stress state all three models are in good agreement, except during the last stage of densification (during this stage model 1 - which represents the experimental results - shows a slower densification rate than the axisymmetric cell models and the Gologanu model). For the triaxiality $X = -4/3$ the Gologanu model gives the highest densification rate.

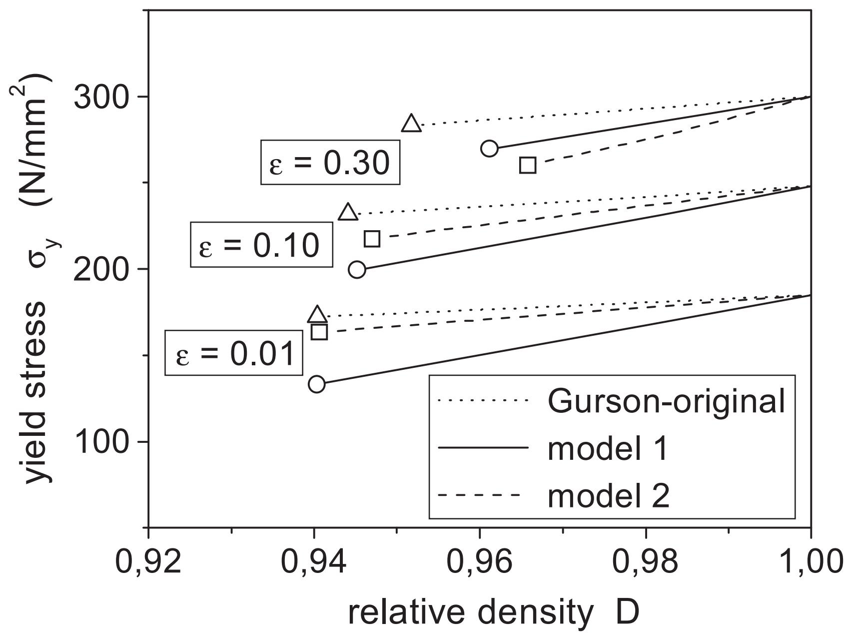

Figure 4. Yield stress of the porous metal versus relative density for different levels of plastic strain; original Gurson model (with $q_1 = q_2 = 1$) compared with the modified Gurson model (model 1) and the Gologanu model (model 2).

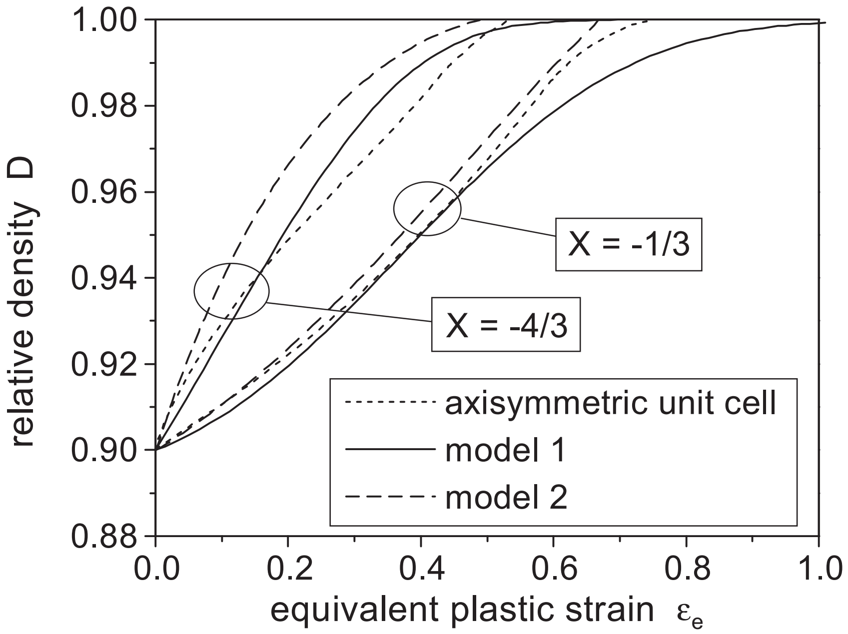

Figure 5. Density evolution for different triaxialities; comparison between axisymmetric unit cell calculations, the modified Gurson model (model 1) and the Gologanu model (model 2).

5. Tapered disk compression

5.1. Forging experiments

In order to subject the two models presented in this paper to a critical test, tapered disk compression experiments were carried out. The initial specimen geometry is shown in figure 6. This test configuration provides a wide range of stress states: in the center of the disk high hydrostatic compressive stresses result in a rapid local densification, whereas tensile stresses at the outer parts lead to a decrease in relative density. Two disks of sintered molybdenum (initial density $D_0 = 0.95$) were deformed with a screw-press. The first stroke reduced the specimen height to $h_1 = 50\,\text{mm}$, the second one to $h_2 = 40\,\text{mm}$. The temperature at the beginning of deformation was $T = 1000^\circ\text{C}$. Samples were cut from each disk after deformation to determine the local density distribution with the Archimedes method. The finite element mesh is depicted in figure 7 together with the contour plots of the experimental and numerical results for the density distribution.

5.2. Numerical results

An isothermal simulation was carried out using axisymmetric conditions with 4 node linear elements. The Coulomb friction factor was taken to be 0.05 between the disk and the rigid dies. This value was obtained from ring upsetting tests. The flow curves for various temperatures and strain rates were also obtained experimentally (Parteder 2000). The parameters of model 1 (equation 7) were defined by the option USER DEFINED FIELD in the ABAQUS input deck, for model 2 a UMAT was developed, as described above. In figure 7 the experimental results can be compared with the predictions of the two models and the original Gurson model (with constant parameters $q_1 = 1.5$ and $q_2 = 1$). On the left column the results for $h_1 = 50\,\text{mm}$ (first stroke) are shown, on the right side results for $h_2 = 40\,\text{mm}$ (second stroke) are depicted.

A comparison of the experimental results and the three models shows, that the modified Gurson model with parameters adjusted to results of hot upsetting tests and cell model calculations (model 1) gives the best consistency with the experiments. Especially in the center of the sample the predicted values are quite reasonable (the relative density in the center obtained from the experiment is $\approx 99.6\,\%$, which is also predicted with model 1). This is not surprising since the triaxiality in the center of the sample is about $X \approx -0.4$, which is close to uniaxial compression for which the parameters were fitted.

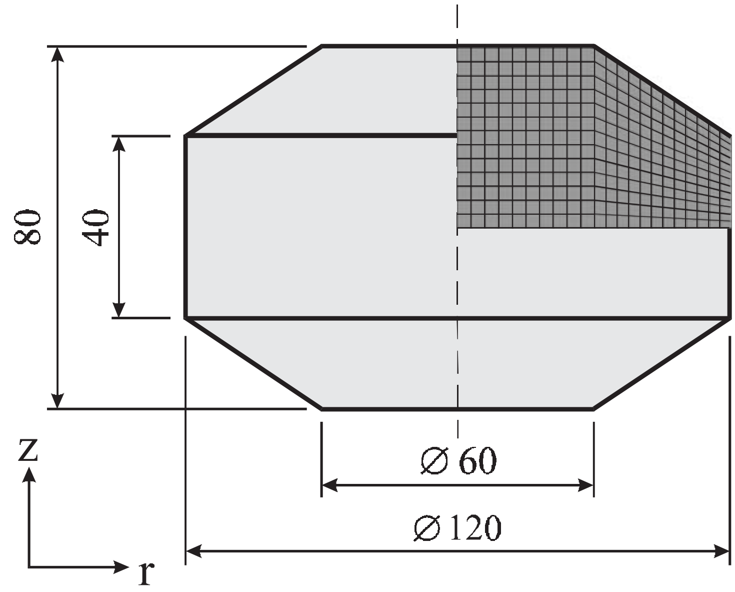

Figure 6. Sketch of the tapered disk sample with finite element mesh.

Also the Gologanu model (model 2) gives density distributions that are generally in good agreement with the experiments. However, the model predicts that the material is completely densified in the center of the sample. This overestimation can be explained looking at figure 5, where the densification in the last stage is more rapid compared with the experimental values. Contrary to the modified Gurson model the Gologanu model contains no adjustable parameters (except the hardening curve of the base material). On the other hand, the original Gurson model gives density distributions that are far less accurate.

Another comparison can be made with the model of Ponte Castañeda (Kailasam et al. 2000). In this case the same tapered disk sample was used and the first stroke was simulated, however with an initial density of $D_0 = 0.85$. In the center of the sample the same tendency as with Gologanu's model can be seen: the final density is overestimated compared to the experimental results.

In figure 8 the pore shape parameter S is plotted for the first stroke calculated with model 2 together with micrographs on four specific positions. In the center (point 1) a value of $S = -6.73$ is predicted, which means a very low pore aspect ratio and therefore an almost fully dense material. The micrograph

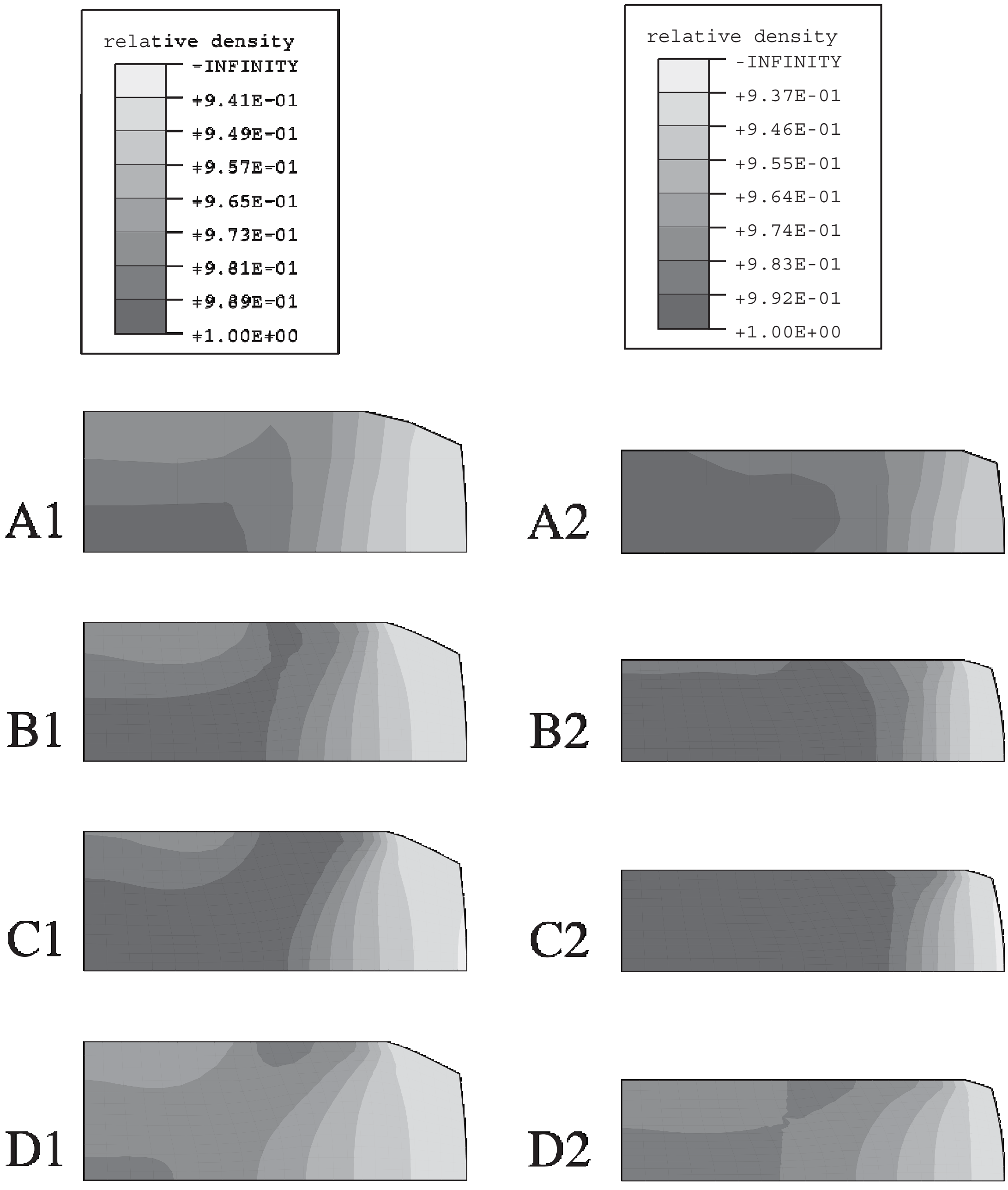

Figure 7. Density distribution for the first stroke (left side: A1 - D1) and for the second stroke (right side: A2 - D2). Comparison of the measured values (A1 and A2), the modified Gurson model (model 1: B1 and B2), the Gologanu model (model 2: C1 and C2) and the original Gurson model (with $q_1 = 1.5$ and $q_2 = 1$) (D1 and D2).

at this position shows little porosity, corresponding to the relative density in figure 7, A1 (experimental value). The aspect ratio calculated at the outer side (point 2) is approximately 1 and is in good accordance to the micrographical observations. At point 3 a value of 0.51 and 0.59 at point 4 resp. is predicted. Also these values are in good coincidation with the micrographs.

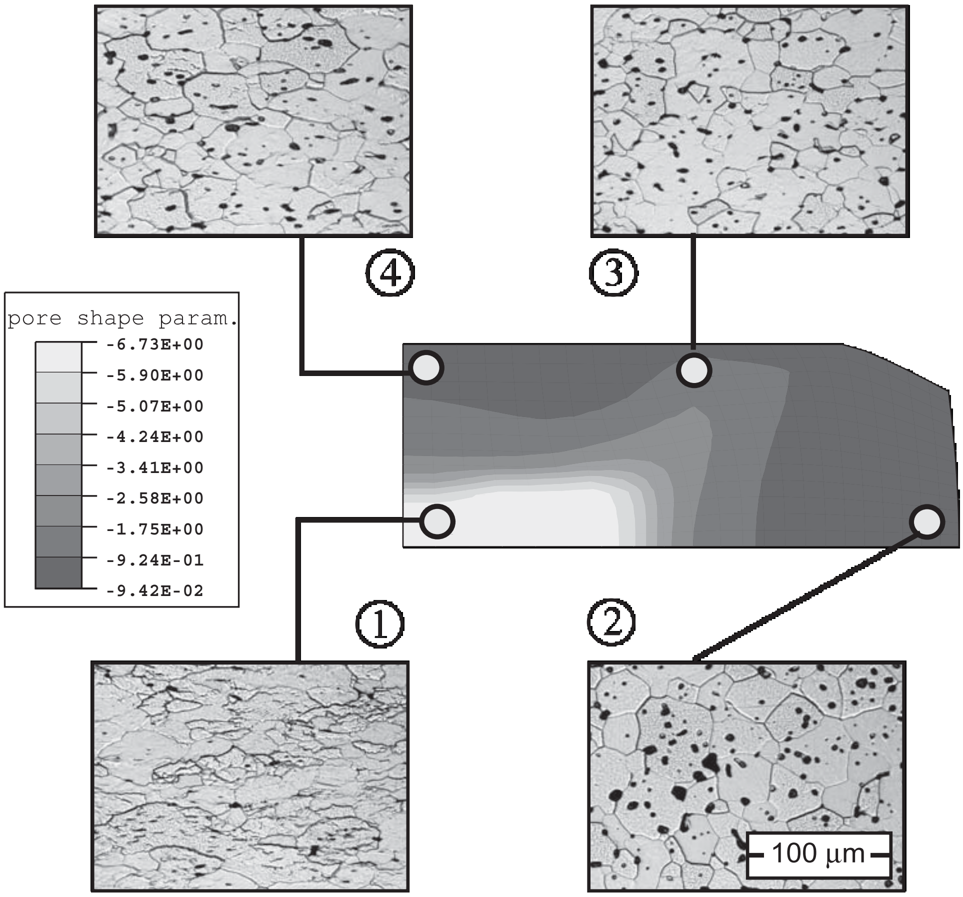

Figure 8. Pore shape parameter S for the first stroke calculated with the Gologanu model (model 2), together with four optical micrographs.

6. Conclusion

The accuracy of predicted density distributions during forming processes of porous metals with closed porosity (up to levels of 10%) can be increased significantly by incorporating the pore shape evolution within the continuum model. Two possibilities were presented in this paper, the first one was a phenomenological modification of the Gurson model, the second one was the model of Gologanu et al. Both models lead to much better results for the density distribution in a tapered disk sample in comparison with the original Gurson model.

References

Andrieux, F., Sun, D.Z., Riedel, H. & Kraft, T. 2000. Verbesserte konstitutive Modelle zur Beschreibung von Umformprozessen. IWM-Bericht Z1/2000, Freiburg: Fraunhofer-Institut für Werkstoffmechanik.

Berg, C.A. 1970. Plastic Dilation and Void Interaction. In Kanninen, M.F. et al. (eds): *Inelastic Behaviour of Solids*: 171-210. London: McGraw-Hill.

Duva, J.M. & Hutchinson, J.W. 1984. Constitutive Potentials for Dilutely Voided Nonlinear Materials. *Mech. Mat.* 3:41-54.

Gologanu, M., Leblond, J.B. & Devaux, J. 1993. Approximate Models for Ductile Metals Containing Nonspherical Voids - Case of Axisymmetric Prolate Ellipsoidal Cavities. *J. Mech. Phys. Solids* 41:1723-1754.

Gologanu, M., Leblond, J.B. & Devaux, J. 1994. Approximate Models for Ductile Metals Containing Nonspherical Voids - Case of Axisymmetric Oblate Ellipsoidal Cavities. *J. Eng. Mat. Technol* 116:290-297.

Gurson, A.L. 1977. Continuum Theory of Ductile Rupture by Void Nucleation and Growth: Part I - Yield Criteria and Flow Rules for Porous Ductile Media. *J. Eng. Mat. Technol.,* 99:2-15.

Kailasam, M., Aravas, N. & Ponte Castañeda, P. 2000. Constitutive models for porous metals with developing anisotropy and applications to deformation processing. *Comp. Mod. in Eng. & Sci.* 1:105-118.

Kuhn, H.A. & Downey, C.L. 1971. Deformation Characteristics and Plasticity Theory of Sintered Powder Materials. *Int. J. Powder Met.* 7:15-25.

Parteder, E., Riedel, H. & Kopp, R. 1999. Densification of Sintered Molybdenum during Hot Upsetting: Experiments and Modelling. *Mat. Sci. Eng.* A264:17-25.

Parteder, E. 2000. *Ein Modell zur Simulation von Umformprozessen pulvermetallurgisch hergestellter hochschmelzender Metalle*. Aachen: Umformtechnische Schriften, Band 94, Shaker Verlag.

Ponte Castañeda, P. & Zaidman, M. 1994. Constitutive Models for Porous Materials with Evolving Microstructure. *J. Mech. Phys. Solids* 42:1459-1497.

Shima, S. & Oyane, M. 1976. Plasticity Theory for Porous Metals*. Int. J. Mech. Sci.* 18:285-291.

Tvergaard, V. 1981. Influence of Voids on Shear Band Instabilities under Plane Strain Conditions. *Int. J. Fract.* 17:389-407.